Lattice design and optimization of the SSRF storage ring with super-bends

TIAN Shun-Qiang (田顺强),[1, *] JIANG Bo-Cheng (姜伯承),[1] ZHOU Qiao-Gen (周巧根),[1]
LENG Yong-Bin (冷用斌),[1] and ZHAO Zhen-Tang (赵振堂)[1]

[1]*Shanghai Institute of Applied Physics, Chinese Academy of Sciences, Shanghai 201800, China*

In the near future, the Phase-II beamline project of Shanghai Synchrotron Radiation Facility (SSRF) will be implemented and some dipoles in the storage ring will be replaced by high field dipoles (super-bend), so as to leave room for short straight sections. In this way, the brightness of the hard x-ray emitted from the super-bends can be enhanced, and more insertion devices can be installed. In this paper, super-bends of two lengths are discussed and the corresponding lattices are presented.

Keywords: Shanghai Synchrotron Radiation Facility (SSRF), Super-bend, Lattice design, Nonlinear optimization

I. INTRODUCTION

Increased user demands for high brightness hard x-rays (20–40 keV) have been seen in recent years, while straight sections to install insertion devices (e.g. superconducting wigglers for hard x-rays) are often limited in a synchrotron radiation light sources. Because the critical photon energy (ε_C, in keV) emitted from dipoles increases with the bending field (B, in T) and beam energy (E_0, in GeV) as $\varepsilon_C = 0.665 E_0^2 B$ [1], much attention is paid to increasing the bending field for high brightness hard x-rays in the synchrotron radiation light sources of moderate beam energy. In the early 1990s, BINP developed a superconducting bending magnet with working field of 6 T, for emitting hard X-rays in a proposed compact synchrotron radiation light source [2]. In 2001, aimed at realizing high brightness hard x-ray production, for the first time ALS replaced three normal dipoles with superconducting bending magnets at a field of over 5 T [3]. This did show a great increase in super-bend availability and capacity.

As shown in Table 1, more and more super-bends are built or proposed at a number of synchrotron radiation light sources (BESSY-II [2], SLS [4], DIAMOND [5], and some low-energy compact rings [6–8]). Besides, SIRIUS [9] in Brazil plans to add a high-field slice in the center of bending magnets so as to reach up to 12 keV of the critical photon energy. Light sources of about 3.0 GeV in beam energy use room temperature bending magnets at about 3 T to reach about 15 keV in the critical photon energy and photon energy of 20–40 keV is available.

The Shanghai Synchrotron Radiation Facility (SSRF), a 3.5 GeV third generation intermediate-energy light source, has been open for users since May 2009 [10, 11]. The SSRF storage ring is based on Double-Bend-Achromatic (DBA) cell [12]. The critical photon energy from the dipoles is about 10.3 keV. By the super-bend replacements, the brightness or flux of the hard X-rays can be significantly enhanced. As an example, Fig. 1 shows that the critical photon energy increases to 24.9 keV with a super-bend of 0.6 m in path length and 3.0543 T in steering field.
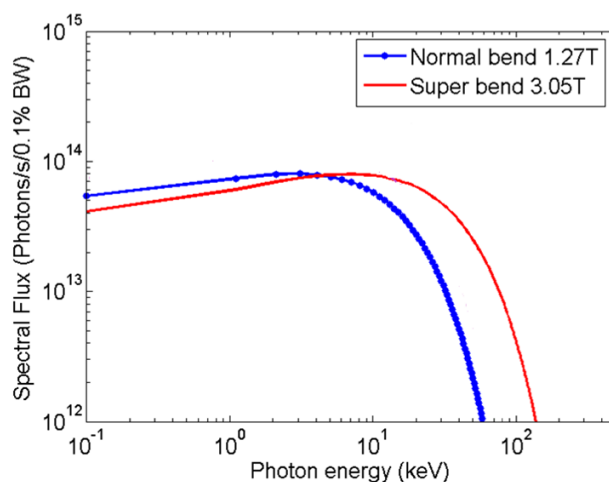
Fig. 1. (Color online) Photon spectrum of normal bend and super-bend (3.05 T) in SSRF.
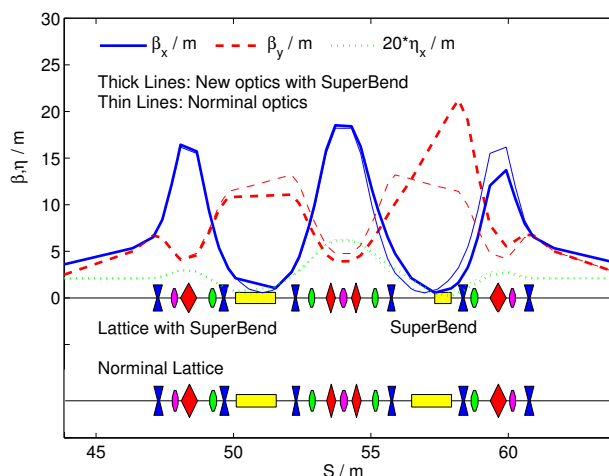

Fig. 2. (Color online) Optics of the single super-bend lattice.

Shortening the dipoles provides a possibility of adding straight sections in the storage ring. By replacing two normal dipoles with two super-bends in one DBA cell, an insertion

TABLE 1.   List of light sources with super-bends (SC, super conducting magnet; RT, room temperature magnet; PM, permanent magnet; NB, normal bend; CJSR, Central Japan Synchrotron Radiation Facility)

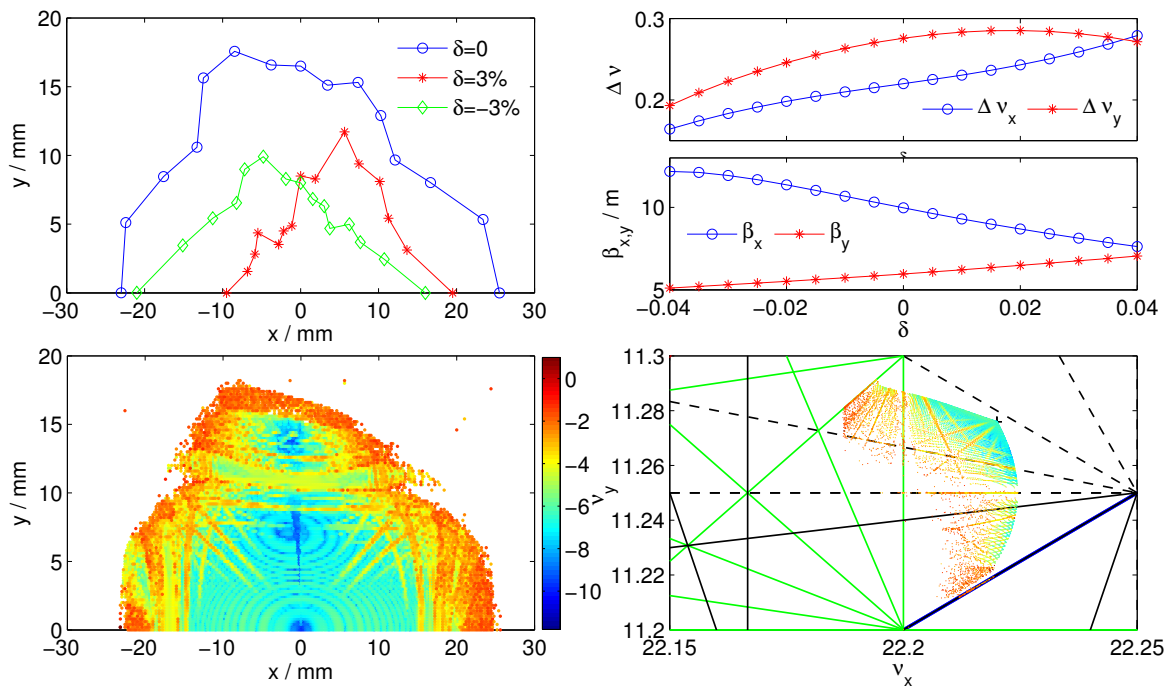| Light source	ALS	BESSY-II	SLS	DIAMOND	SIRIUS	BINP's	CJSR
Beam energy /GeV	1.9	1.7	2.4	3.0	3.0	1.2	1.2
Circumference /m	196.8	240	288	561.6	~ 460	<60	72
Super-bend field /T	5.0	8.5	2.9	3.0	2.0	8.5	5
Super-bend number	3	4	3	1 (proposed)	~ 20	6	4
Super-bend type	SC	SC	RT	RT	PM	SC	SC
Critical photon energy /keV	12	16.3	11.1	18	12	8.1	4.8
NB field /T	1.3	1.53	1.4	1.4	0.5	1.65	1.4
Criti. energy from NB /keV	3.1	3.7	5.4	8.4	3.0	1.6	1.34

Fig. 3. (Color online) Dynamic aperture, frequency maps, β function variation and tune shift of the single super-bend lattice.

TABLE 2.   Beam parameters of different schemes (S-B, super-bend; LSS, long straight section; SSS, standard straight section; NSS, new straight section) at 3.5 GeV of beam energy and 200 mA of beam current

Parameter /unit	Present Lattice	Single S-B	Eight 0.6 m-S-B	Eight 0.8 m-S-B
Circumference /m	432	431.9965	431.9719	431.9785
Beam energy /GeV	3.5	3.5	3.5	3.5
Beam current /mA	200	200	200	200
Tune (H, V)	22.22, 11.29	22.22, 11.276	23.23, 11.31	23.23, 11.31
Natural emittance /nm.rad	3.89	4.07	3.62	3.51
RMS energy spread	0.0010	0.0010	0.0012	0.0011
Effect. Emit. @ LSS	4.863	5.114	4.550	4.286
Effect. Emit. @ SSS	5.170	5.433	5.292	4.915
Effect. Emit.@ NSS	—	—	5.294	5.165
Natural Chrom. (H, V)	$-55.67, -17.95$	$-55.49, -18.14$	$-75.30, -22.53,$	$-71.50, -22.02$
Energy loss per turn /MeV	1.435	1.486	1.844	1.670
Damp. time (H, V, L) /ms	7.05, 7.02, 3.51	6.80, 6.78, 3.39	5.48, 5.47, 2.73	6.05, 6.04, 3.01
Mom. Compact. Factor	4.27×10^{-4}	4.19×10^{-4}	3.60×10^{-4}	3.64×10^{-4}
RF voltage /MV	4.2	4.2	4.2	4.2
RF frequency /MHz	499.654	499.658	499.687	499.679
Harmonic number	720	720	720	720
Synchrotron frequency	0.00743	0.00734	0.00667	0.00678
Natural bunch length /ps	13.2	13.1	15.1	13.5

device can be installed at the cell center, as in the SOELIL lattice [13]. The number of ID straight sections is limited in
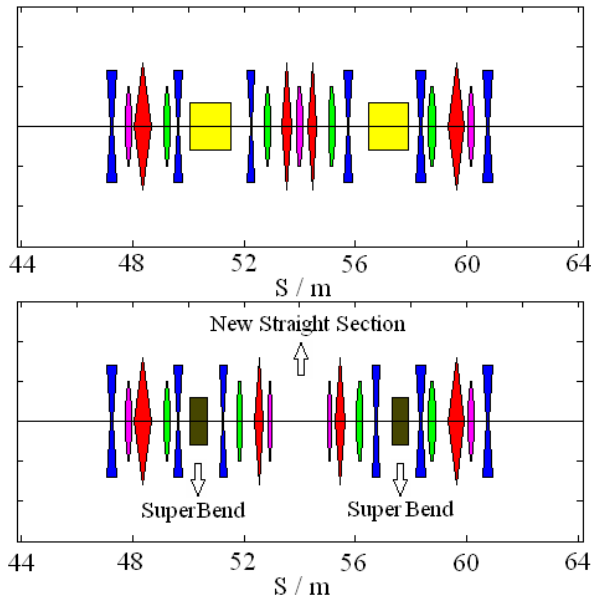
Fig. 4. (Color online) DBA cell reconstruction and their locations in the SSRF storage ring.

SSRF, and a detailed study of this scheme is done for the SSRF phase-II beamline project. The machine performance is maintained as good as possible with the current hardware, such as the RF capability, maximum strength of the quadrupole and the sextupole.
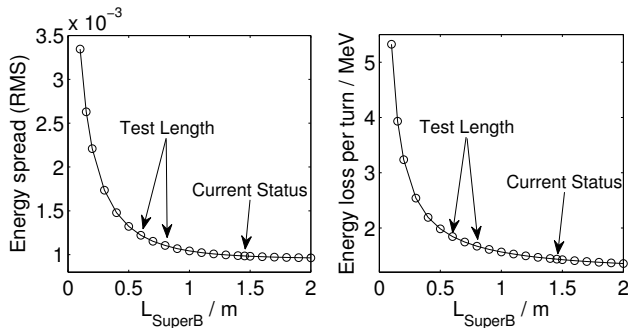

Fig. 5. Energy spread and energy loss per turn as a function of the path length in the super-bend.

The challenges in the super-bend approach of SSRF include 1) lattice design and beam dynamics optimization for maintaining machine performance; 2) design, fabrication, and installation of the super-bend; 3) associated need to control errors in field and the alignment; 4) instability of the power supply, which can induce orbit jitter and beam energy vibration; 5) possible changes to the vacuum system; and 6) increase of the beam energy loss and the compensation capability of the RF system. In this paper, we report the results about the lattice design and beam dynamics, and a preliminary design of the super-bend. The cases of a single super-bend and eight super-bends are discussed in Sec. II and Sec. III, respectively, and a preliminary design for super-bend magnet is given in Sec. IV.

II. SINGLE SUPER-BEND LATTICE

At first, one normal dipole in the central DBA cell of a super-period in the storage ring is replaced by a super-bend of $0.6\,\mathrm{m}$ in beam path and $3.0543\,\mathrm{T}$ in steering field. The ten quadrupoles in this cell are individually adjusted for optics matching. The matching process keeps all the linear optical parameters of the source points, including β_x, β_y, η and their divergences. Because of the periodicity degeneration, a nonlinear resonance becomes stronger nearby the nominal working point of 22.220 (H) and 11.290 (V), which shifts to 22.220 (H) and 11.276 (V). Fig. 2 plots the linear optics and shows the lattice change in this cell. The beam parameters are summarized in Table 2. Fig. 3 shows the re-optimized nonlinear dynamics, including on- and off-momentum dynamic apertures, frequency maps [14–16], beta function variation, and tune shift with energy deviation. The chromaticity is corrected to 1 in both transverse planes, and the other cases are of the same. The natural emittance and energy spread increase a little, and the effective emittance along the ring increases by 5% with respect to the nominal optics. The beam energy loss per turn increases by about 4%, which can be compensated easily by the current RF system. Degradation of the dynamic acceptance is due to the symmetry broken. However, this solution is of the high injection efficiency and long beam lifetime.

III. EIGHT SUPER-BEND LATTICE

As shown in the left of Fig. 4, by replacing the two dipoles in a DBA cell with the super-bends, and making the magnets in the arc close to the super-bends, an additional straight section is formed. We propose to replace eight normal dipoles in four DBA cells to form four more straight sections (Fig. 4 in the right). The new straight section should be longer than 2 m (the
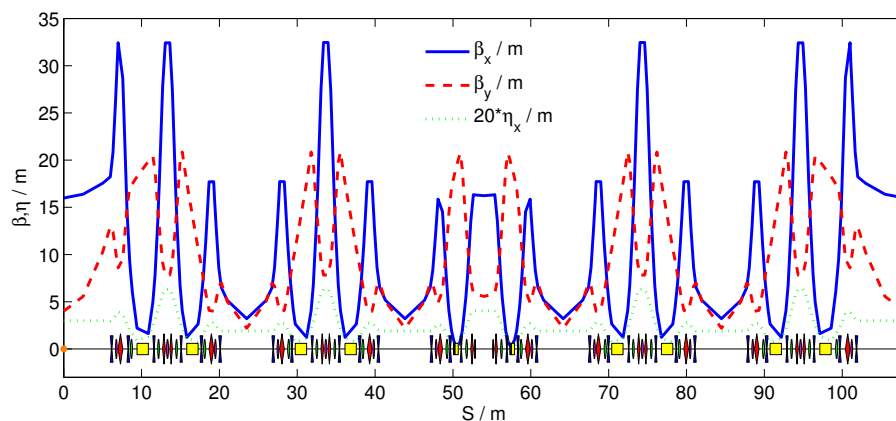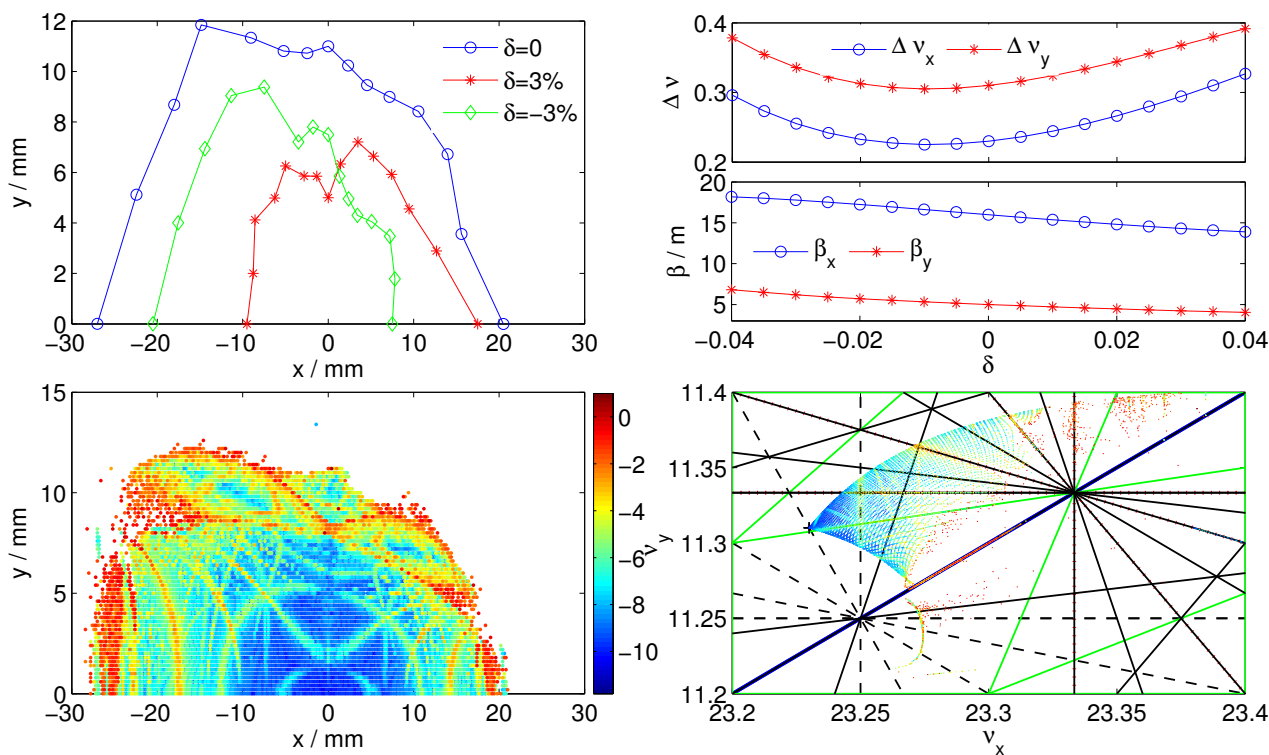
Fig. 6. (Color online) Linear optics of one super-period in the 0.6 m-length super-bend lattice.

Fig. 7. (Color online) Dynamic aperture, frequency maps, β variation and tune shift of the 0.6 m-length super-bend lattice.

longer, the better) for installing a short insertion device.

Figure 5 plots the energy spread and the energy loss per turn as a function of the beam path length in the super-bend in this case. At the beam current of 300 mA, the RF system can support ~ 2 MeV per turn of the energy loss, which includes radiation from dipoles and IDs. So, the beam path length in the super-bend must be longer than 0.5 m. The energy spread has a component of the effective emittance in the source point [17, 18]. For a high photon brightness, it should be low enough. The super-bend path length of 0.6 m and 0.8 m are considered (Fig. 5). The 0.8 m-length super-bend has a steering field of 2.2907 T, with the critical photon energy of 18.7 keV.

When the working points are the same as the nominal one, the natural emittance increases up to about 5 nm rad in the 0.6 m-length super-bend lattice. Due to the large energy spread and natural emittance, the effective emittance increases by about 40% with respect to the nominal optics. The brightness decreases with increasing effective emittance. To avoid this, the horizontal working point is increased by one unit. The horizontal beta function at the injection point increases to 16 m in order to get sufficient dynamic aperture. Fig. 6 plots the linear optics and Fig. 7 gives the nonlinear optimal results. The beam parameters are summarized in Table 2. The natural emittance is 3.62 nm rad, and the effective emittance in the standard straight section is 5.29 nm rad, being just 2% higher than the
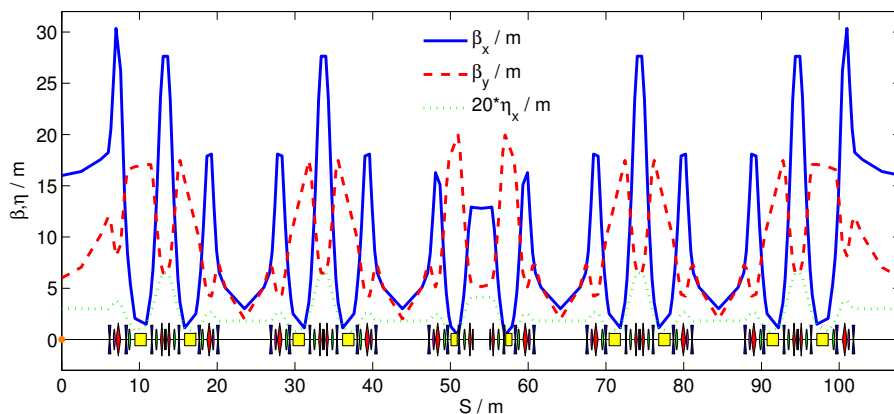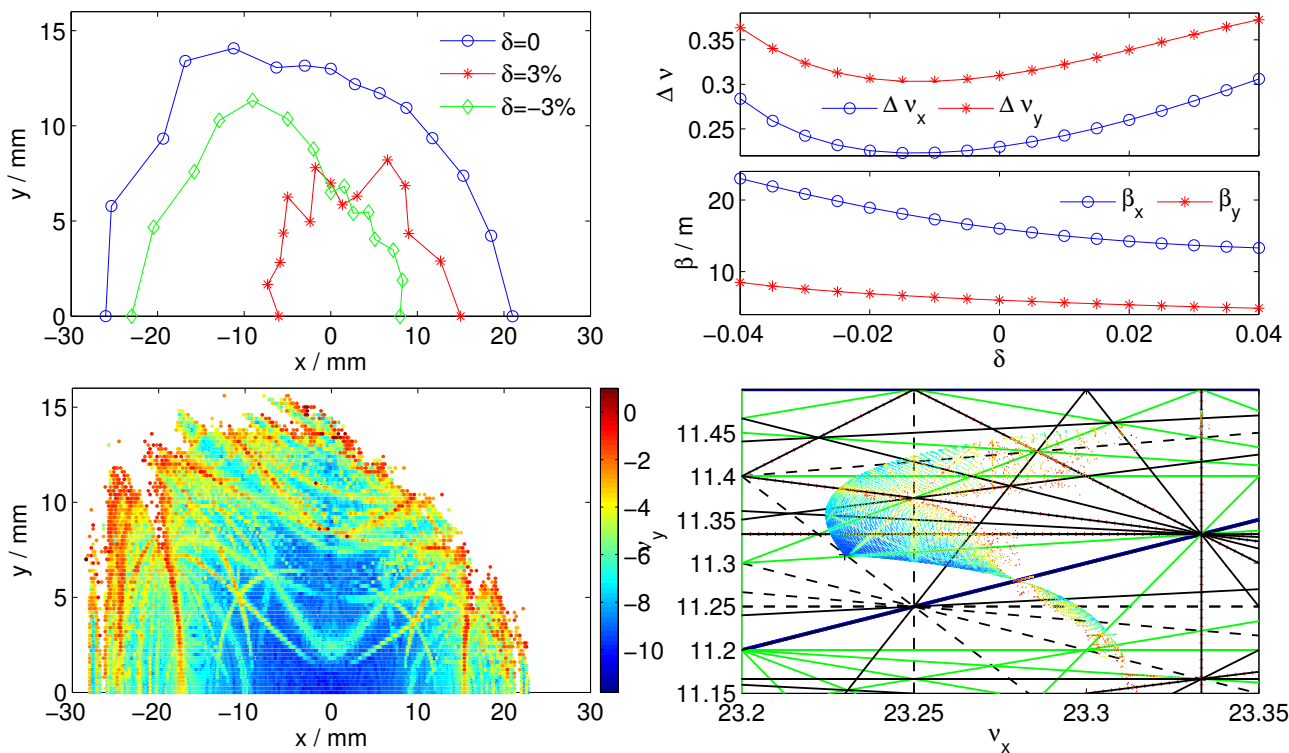
Fig. 8. (Color online) Linear optics of one super-period in the 0.8 m-length super-bend lattice.

Fig. 9. (Color online) Dynamic aperture, frequency maps, β variation and tune shift of the 0.8 m-length super-bend lattice.

nominal optics. The dynamic aperture is sufficient to reach high injection efficiency.

The large energy loss per turn in the 0.6 m-length super-bend lattice makes it difficult to store 300 mA beam current on the current RF system, as the SSRF storage ring has many insertion devices. Using the 0.6 m-length super-bend lattice, the beam energy shall be 3.0 GeV, rather than 3.5 GeV, while using the 0.8 m-length super-bend lattice, the energy loss per turn is just 1.670 MeV at 3.5 GeV. Fig. 8 plots the linear optics in one super-period and and Fig. 9 gives the nonlinear optimal results. The beam parameters are summarized in Table 2. The working point of this lattice is 23.23 (H), 11.31 (V), the same

as the 0.6 m-length super-bend lattice. The natural emittance is 3.51 nm rad, and the effective emittance in standard straight section is reduced to be 4.915 nm rad. The frequency maps show a resonance-free interior part in the dynamic aperture, which is beneficial to reach high injection efficiency.

IV. PRELIMINARY MAGNET DESIGN FOR SUPER-BEND

All of the three schemes of the super-bend are of nice beam dynamics, being applicable in machine operation. The 0.8 m-length super-bend lattice is easy to keep the effective emittance
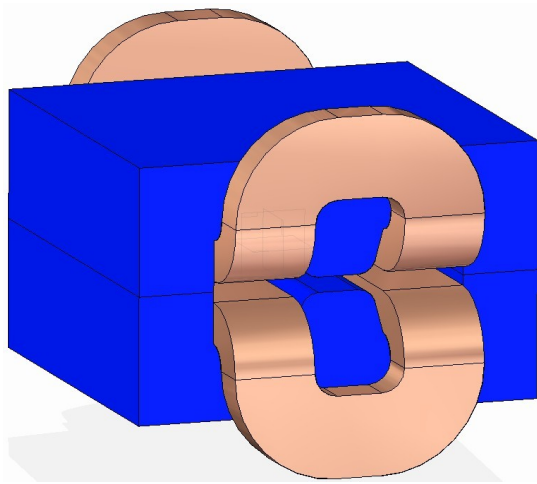
Fig. 10. (Color online) General view of the super-bend design.

±18 mm, which is appropriate to the machine operation with the upgraded lattice.

TABLE 3. Main parameters of super-bend

Parameter /unit	Value
No. of super-bend	8
Peak field /T	2.4
Good field region /mm	±18
Deflection angle	9
Pole gap /mm	30
Pole length (Z), width (X), height (Y) /mm	750, 800, 500
No. of coil turn	36
Conductor cross-section /mm	$16 \times 16\Phi7$
Current /A	1050.43
Voltage /V	19.2
Power /kW	20.2

and the photon brightness from IDs as the nominal one, and the energy loss per turn is moderate to the current RF system at 3.5 GeV, hence a good scheme for the SSRF lattice upgrade.

However, due to the limited space for the super-bend, it is difficult to design a super-bend with good field quality. A super-bend can be a permanent magnet, superconducting magnet, or electromagnet. A permanent magnet suffers from demagnetization by beam loss, and corresponding nonuniformity among the super-bends. A superconducting magnet, which is expensive, is not necessary for a steering field of just 2∼3 T for the SSRF storage ring. Therefor, an electromagnet is still a good option. Fig. 10 shows a preliminary magnet design with H-frame yoke, and Table 3 summarizes the main parameters. The peak field is 2.4 T, and the good field region is about

V. CONCLUSION

Different schemes of the lattice upgrade at SSRF with the super-bend are discussed. They include single super-bend lattice, eight 0.6 m- and 0.8 m-length super-bend lattice. The single super-bend lattice focuses on the usage of high photon brightness, while the eight super-bend lattice schemes provides four short straight sections of 2 m length, which is attractive to SSRF. The 0.6 m-length super-bend lattice suffers from high energy loss per turn, and is appropriate at 3.0 GeV beam energy. The 0.8 m-length super-bend lattice is a better solution in the current conditions, and a preliminary magnet design for this scheme is presented. After careful optimization, the beam emittance of all the three schemes is very close to the nominal one, and the dynamic acceptance can fulfill efficient injection and long beam lifetime.

[1] Chao A W. Handbook of Accelerator Physics and Engineering, 1999 **208**: World Scientific.

[2] Batrakov A M, Khruschev S V, Kraemer D, *et al.* Nucl Instrum Methods Phys Res A, 2005, **543**: 35–41.

[3] Robin D, Krupnick J, Schlueter R, *et al.* Nucl Instrum Methods Phys Res Sect A 2005, **538**: 65–92.

[4] Gabard A, George D, Negrazus M, *et al.* in Proceedings of IPAC2011, San Sebastian, Spain, 2011, 3038–3040.

[5] Walker R P, Bartolini R, Cox M P, *et al.* in Proceedings of IPAC2011, San Sebastian, Spain, 2011, 3059–3061.

[6] Antokhin E I, Gvozdev A A, Kulipanov G N, *et al.* in Proceedings of APAC 2007, Indore, India, 127–129.

[7] Antokhin E I, Gvozdev A A, Kulipanov G N, *et al.* Nucl Instrum Methods Phys Res A, 2007, **575**: 1–6.

[8] Yamamoto N, Takashima Y, Hosaka M, *et al.* in Proceedings of IPAC2011, San Sebastian, Spain, 2011, 2987–2989.

[9] Liu L, Basilio R, Citadini J F, *et al.* in Proceedings of IPAC2011, San Sebastian, Spain, 2011, 931–933.

[10] Xu H J and Zhao Z T. Nucl Sci Tech, 2008, **19**: 1–6.

[11] Zhao Z T, Xu H J, Ding H. in Proceedings of PAC09, Vancouver, BC, Canada, 2009, 55–57.

[12] Liu G M, Dai Z M, Li H H, *et al.* High Energy Physics and Nuclear Physics, 2006, **30**, Supp. I, 144–146.

[13] Nadji A, Besson J C, Betinelli P, *et al.* in Proceedings of EPAC2006, Edinburgh, Scotland, 2006, 3284–3286.

[14] Laskar J. in Proceedings of PAC2003, Portland, USA, 2003, 378–382.

[15] Robin D, Steier C, Laskar J, *et al.* Phys Rev Letters, 2000, **85(3)**: 558–561.

[16] Nadolski L and Laskar J. Phys Rev Special Topics A&B, 2003, **6**: 114801.

[17] Tanaka H and Ando A. Nucl Instrum Methods Phys Res Sect A, 1996, **369**: 312–321.

[18] Lee S Y. Phys Rev E, 1996, **54(2)**: 1940–1944.